Title

Integration of image exposure time into a modified laser speckle imaging method

Permalink

Journal

Physics in Medicine and Biology, 55(22)

ISSN

0031-9155

Authors

Ramírez-San-Juan, JC
Huang, YC
Salazar-Hermenegildo, N
et al.

Publication Date

2010-11-21

DOI

10.1088/0031-9155/55/22/016

Copyright Information

Peer reviewed

Integration of image exposure time into a modified laser speckle imaging method

J C Ramírez-San-Juan[1], **Y C Huang**[2,3,4], **N Salazar-Hermenegildo**[1], **R Ramos-García**[1], **J Muñoz-Lopez**[1], and **B Choi**[3,4,5]

J C Ramírez-San-Juan: jcram@inaoep.mx

[1]Optics Department, INAOE, Puebla, Mexico

[2]Department of Electrical Engineering and Computer Science, University of California, Irvine, CA, USA

[3]Beckman Laser Institute and Medical Clinic, University of California, Irvine, CA, USA

[4]Department of Biomedical Engineering, University of California, Irvine, CA, USA

[5]Edwards Lifesciences Center for Advanced Cardiovascular Technology, University of California, Irvine, CA, USA

Abstract

Speckle-based methods have been developed to characterize tissue blood flow and perfusion. One such method, called modified laser speckle imaging (mLSI), enables computation of blood flow maps with relatively high spatial resolution. Although it is known that the sensitivity and noise in LSI measurements depend on image exposure time, a fundamental disadvantage of mLSI is that it does not take into account this parameter. In this work, we integrate the exposure time into the mLSI method and provide experimental support of our approach with measurements from an *in vitro* flow phantom.

1. Introduction

Fercher and Briers (1981) proposed a method for flow visualization by means of single-exposure photography. This method employs the spatial statistics of time-integrated speckle (essentially the speckle contrast) and was originally developed for the measurement of retinal blood flow. It is essentially a spatial extension of dynamic light scattering principles (Bandyopadhyay *et al* 2005). This laser speckle imaging (LSI) (Boas and Dunn 2010) method has evolved into a digital, real-time approach for blood flow mapping (Briers and Webster 1995, Briers *et al* 1999, Liu *et al* 2008, Tom *et al* 2008). LSI has been used to monitor noninvasively blood flow and perfusion dynamics in the brain (Dunn *et al* 2001, 2005, Cheng *et al* 2003, 2004, Yuan *et al* 2005, Bolay *et al* 2002, Ayata *et al* 2004, Durduran *et al* 2004, Zhou *et al* 2008), retina (Fercher and Briers 1981, Hirao *et al* 2004) and skin (Forrester *et al* 2004, Choi *et al* 2004, 2006, 2008, Smith *et al* 2006). We have employed this method to monitor chronic blood flow dynamics during photodynamic therapy (Smith *et al* 2006, Choi *et al* 2008) and pulsed laser irradiation (Choi *et al* 2008, Jia *et al* 2007, 2010, Huang *et al* 2009) and have observed marked changes in the measured speckle flow index (SFI) values.

A disadvantage of spatial speckle contrast analysis is the degradation in spatial resolution that results from quantitative analysis of local speckle contrast from a subregion of camera pixels, typically 5×5 or 7×7. To address this issue, Cheng *et al* (2003, 2008) developed a modified LSI (mLSI) method that analyzes the temporal statistics of time-integrated speckle. This mLSI method involves analysis of the temporal information collected at individual

camera pixels, and hence enables study of blood flow dynamics in smaller blood vessels. mLSI preserves the original spatial resolution by sacrificing the temporal resolution (Le *et al* 2007).

A fundamental disadvantage of mLSI is that it does not take into account the camera exposure time. It is well known that the sensitivity and noise in the measurement of blood flow changes depend on exposure time (Briers and Webster 1995, Briers *et al* 1999, Yuan *et al* 2005, Choi *et al* 2006, Parthasarathy *et al* 2008).

In this paper, we first incorporate the exposure time into the mLSI equation. We then discuss the need to include image exposure time to expand the linear response range of mLSI, and we describe a general rule-of-thumb to guide selection of image exposure time. Data from *in vitro* experiments are presented to demonstrate empirically the need to consider image exposure time and the improved quantitation of relative flow changes with use of two exposure times.

2. Theory

Cheng *et al* (2003) utilized the first-order temporal statistics of time-integrated speckle to obtain a 2D distribution of blood flow. With their mLSI method, the mean velocity of the scattering particles of the flow is inversely proportional to the parameter N_t:

$$1/N_t = \langle I \rangle^2 / (\langle I^2 \rangle - \langle I \rangle^2), \tag{1}$$

where $\langle I \rangle$ and $\langle I^2 \rangle$ are the mean and mean-square values, respectively, of time-integrated speckle intensities during the time interval t for a specific pixel.

Recently, the same authors demonstrated that the equations for mLSI and spatial LSI have the same form and showed that (Cheng and Duong 2007, Cheng *et al* 2008)

$$1/N_t = 1/K_t^2, \tag{2}$$

where K_t is the 'temporal' contrast.

From Goodman's theory on integrated intensity (Goodman 1985), it is straightforward to obtain (Ramirez-San-Juan *et al* 2008)

$$\frac{1}{K_t^2} \equiv \frac{\langle I \rangle^2}{\langle I^2 \rangle - \langle I \rangle^2} = \left(\frac{\tau_c}{T} + \frac{1}{2} \left(\frac{\tau_c}{T} \right)^2 [e^{-2(T/\tau_c)} - 1] \right)^{-1}. \tag{3}$$

For the Lorentzian spectrum approximation, where $\langle I \rangle$ and $\langle I^2 \rangle$ are defined as in equation (1), T is the integration time and τ is the correlation time. The second term in equation (3) is, in fact, the parameter $1/N_t$ defined in equation (1); therefore,

$$\frac{1}{N_t} = \left(\frac{\tau_c}{T} + \frac{1}{2} \left(\frac{\tau_c}{T} \right)^2 [e^{-2(T/\tau_c)} - 1] \right)^{-1}. \tag{4}$$

For $T \gg \tau_c$, equation (4) becomes

$$1/N_t = T/\tau_c. \tag{5}$$

From equation (5), it is clear that the physical meaning of the parameter $1/N_t$ is the number of coherence intervals captured during the exposure time T. However, there are multiple combinations of velocity and T that yield the same value of $1/N_t$. Also from equation (5), the physical meaning of the speckle flow index (SFI $\equiv 1/\tau_c$) is the rate of coherence intervals captured over unit time:

$$SFI \equiv 1/\tau_c = 1/TN_t. \tag{6}$$

Equation (6) is similar to equation (2), with the important difference that it accounts for image exposure time so that the target range of velocity sensitivity can be varied.

Incorporation of the exposure time to the mLSI method is particularly useful when the blood flow speeds in the field of view are expected to span a wide range of values. A large dynamic range would be necessary to study blood flow dynamics in vessels of different type, as well as in response to flow-modulating stimuli (i.e. photocoagulation, vasoactive drugs, etc). Since LSI is typically used to estimate relative changes in blood flow, it is important to operate in the linear response range of LSI. The flow speeds contained within this range depend on the image exposure time (Choi *et al* 2006). We propose that judicious use of multiple exposure times can be used to expand the linear response range of LSI. With the conventional mLSI method (equation (2)), this expansion cannot be performed; however, with the use of equation (6), multiple exposure times can be used in an automated fashion, as we will now demonstrate.

We now must address the following practical question: How does an end user know that multiple image exposure times may be required during data analysis to operate continuously in the linear response range of each exposure time? Yuan *et al* (2005) defined the sensitivity of LSI to relative changes in flow rate as the ratio of the relative speckle contrast change to the relative flow speed change:

$$S_r = \left| \frac{\frac{dK}{K}}{\frac{dv}{v}} \right| = -\frac{r}{K}\frac{dK}{dr} = \frac{1}{2K^2r^2}[r-1+(r+1)\,e^{-2r}], \tag{7}$$

where K is the speckle contrast given by

$$K = \left(\frac{1}{r} + \frac{1}{2}\left(\frac{1}{r^2}\right)(e^{-2r}-1) \right)^{1/2} \tag{8}$$

and $r = T/\tau_c$ is the number of coherent intervals captured per unit time (i.e. $1/N_t$). From figure 1, we can see that S_r reaches an asymptotic value of 0.5 for values of r greater than ~50. Hence, for $r > 50$, the relative speckle contrast response is proportional to the actual relative change in flow speed (Yuan *et al* 2005). Our experimental data (figure 2(a)) support this statement, as we observe that a linear response range is achieved for $r = 1/N_t > 50$.

Hence, to determine the optimal image exposure time to use in analysis of relative flow rate changes assessed with LSI, the end user should calculate relative flow rate changes only if the data sets satisfy the $r \geq 50$ criterion. This rule-of-thumb applies to both mLSI and spatial LSI data. Our experimental data (see section 4 below) support this rule-of-thumb.

For an image in which multiple flow speeds are encountered (i.e. microvasculature in a cranial or dorsal window chamber preparation), ideally one would collect sequences of images at multiple exposure times and, with analysis of the ensuing $1/N_t$ maps identify the optimal exposure-time images to use to analyze relative blood flow changes for each pixel. In many experimental scenarios for which high temporal resolution is not required (i.e. cortical spreading depression following focal cerebral ischemia), this approach is viable.

3. Experimental design

3.1. LSI instrument

We used an instrument described previously in the literature (Choi *et al* 2006). The instrument consisted of a 30 mW, 633 nm He-Ne laser, plano-convex lens, beam steering mirrors, digital charge-coupled device (CCD) camera equipped with a macro lens and desktop personal computer (PC). Collimated light emitted from the laser became divergent after passing through the plano-convex lens. To make the instrument more compact, mirrors were used to steer the diverging beam to the target plane. The resultant speckle pattern was imaged on the CCD array at 1:1 magnification and acquired to the PC memory. The f-stop of the camera lens was set to achieve a sampling rate of two pixels per minimum speckle size (Kirkpatrick and Duncan 2008).

3.2. In vitro flow phantom

The phantom preparation protocol was similar to that described previously (Choi *et al* 2006). To generate scattering agar gels, we boiled a solution consisting of 100 mL of deionized water and 10 mL of glycerol. The latter was used to improve the mechanical integrity of the resultant gels. We added simultaneously 0.3 g of TiO_2 and 2 g of agar to the boiling solution. The former was used to increase the scattering coefficient of the otherwise clear gels, and the agar added was deemed appropriate to simulate the reduced scattering coefficient of the skin. The solution was then poured into various molds (e.g., Petri dishes, sandwiched glass slides) to achieve the desired thickness (150 μm to several millimeters) and allowed sufficient time to solidify. In specific gels, a 550 μm inner-diameter glass capillary tube was embedded into the mold prior to solidification. A syringe-based infusion pump was used to inject fluid into the flow tube. Tygon tubing delivered the fluid from the filled syringe mounted on the pump to the tube embedded in the gel. Intralipid (1% concentration) was used as the fluid in this study.

3.3. Experiments

The infusion pump was set to achieve flow rates of up to 13 mm s^{-1}. The flow phantom was imaged with the LSI instrument. Image exposure times of 0.1, 1 and 10 ms were selected as representative values based on those used in previous studies (Choi *et al* 2004, Dunn *et al* 2005, Yuan *et al* 2005).

3.4. mLSI image analysis

The mLSI algorithm has been described previously in detail (Cheng *et al* 2003). Briefly, the value N_t of each pixel in m consecutive images of the raw speckle pattern was computed according to equation (1). Data were rendered as two-dimensional false-color-coded maps which displayed the spatial variation of the flow speed distribution in the region of interest.

4. Results

The primary objectives of this paper are to illustrate the need to include the image exposure time in mLSI (equation (1)) and to validate the resultant speckle imaging equation (6). To

this end, we developed two sets of *in vitro* flow experiments employing the experimental setup described above.

4.1. Camera exposure time needs to be considered with mLSI analysis

In the first set of experiments we varied the actual flow rate between 1 and 13 mm s^{-1}. For these experiments, image exposure time was held constant at $T = 1$ ms. To calculate values for mean SFI and $1/N_t$ as a function of the actual flow rate, we selected a 300×100 subregion of pixels within the tube and calculated the corresponding mean values for each actual flow rate values and the standard deviation of the mean values. A linear relationship between values of SFI and flow rates between 5 and 13 mm s^{-1} was observed (figure 2(a)), indicating that $T = 1$ ms is an appropriate exposure time for this range of flow rates. However, for flow rates below 5 mm s^{-1}, SFI values deviated from the linear fit, suggesting that $T = 1$ ms was too short to maintain the linear relationship.

In a subsequent set of experiments, we varied the actual flow rate between 0.5 and 6 mm s^{-1} with an image exposure time of $T = 10$ ms. A longer exposure time was used to shift the linear response range of LSI to slower flow rates (Choi *et al* 2006). We observed a linear relationship for both parameters (SFI and $1/N_t$), suggesting that $T = 10$ ms is appropriate to maintain a linear response over this range of flow rates (figure 2(b)).

From the physical meaning of the parameter $1/N_t$, multiple combinations of T and actual flow rate can produce the same $1/N_t$ value (figure 3(a)). For example, consider a $1/N_t$ value of 100. Based on the data in figure 2, it is clear that this value will map to different actual flow rate values, depending on which image exposure time is used. Specifically, this value corresponds to either ~11 mm s^{-1} ($T = 1$ ms, figure 2(a)) or ~0.8 mm s^{-1} ($T = 10$ ms, figure 2(b)). In contrast, the SFI value is unaffected by a change in exposure time (figure 3(b)).

Collectively, these data demonstrate that the linear response range of $1/N_t$ values obtained with the mLSI method is affected by the image exposure time. This result is in agreement with previous findings (Choi *et al* 2006) and justifies the need to include the image exposure time in the mLSI imaging equation (1) and to validate the resultant imaging equation (5).

4.2. Incorporation of the exposure time in the mLSI model improves substantially the accuracy of this method to measure relative flow rate changes

We now calculate the relative flow rate change predicted with the mLSI model ($1/N_t$, equation (1)) and our proposed model (SFI, equation (6)). To do this, we acquired speckle flow images from the above-described *in vitro* flow phantom at two actual flow rates of 3 and 10 mm s^{-1}. As a thought experiment envision the initial flow rate to be 10 mm s^{-1} that decreased to 3 mm s^{-1} due to an intervention (i.e. laser, stimuli, drug, etc). Figure 4 shows the flow rate maps predicted with the mLSI model (equation (1)).

Figure 5 shows the SFI maps predicted with our model (equation (6)) for the same flow rates (10 and 3 mm s^{-1}). Since equation (5) allows for the consideration of image exposure time, both images were acquired in the linear response ranges of their corresponding exposure times, $T = 1$ and 10 ms, respectively (see figure 2).

To calculate the relative flow rate changes predicted by $1/N_t$ and SFI from figures 4 and 5, respectively, we selected a 300×100 subregion of pixels within the tube and then calculated the corresponding mean values (table 1). The actual relative flow rate change was 3.33. The conventional mLSI model (equation (1)) predicted a relative flow rate change of 5.2, and our model (equation (6)) predicted a relative flow rate change of 3.16, or a relative error of 56.15% and 5.1%, respectively.

In table 2, we calculated the relative flow rate change for an additional thought experiment in which the initial flow rate of 9 mm s^{-1} is assumed to decrease to 2 mm s^{-1}.

For the second example, the actual relative flow rate change was 4.5. The conventional mLSI model predicted a relative flow rate change of 17.01, and our model a change of 3.37, or a relative error of 278% and 25.1%, respectively.

An unexpected finding was the large difference in relative errors observed in the two separate experiments summarized in tables 1 and 2 (5% and 25%, respectively). We propose that the fivefold difference in relative error, may be due in part to the complex motion we anticipate, may exist during our experiments, especially at low flow rates. At these flow rates, the relative degree of Brownian motion and ordered motion is unknown, and therefore a more realistic model may be required (Duncan and Kirkpatrick 2008). Further study is warranted. Nevertheless, despite the difference in relative errors, data from both experiments strongly support our central hypothesis that exposure time must be integrated into the conventional mLSI algorithm to improve its accuracy by as much as one order of magnitude.

In conclusion, based on Goodman's theory of time-integrated intensity of thermal or pseudothermal light, we have incorporated the image exposure time into the mLSI equation, resulting in equation (6). We have validated our approach with experimental data collected from an *in vitro* flow phantom. Use of equation (6) over the conventional mLSI equation (2) enables a substantial improvement in the accuracy of assessing flow rate changes using mLSI.

Acknowledgments

References

Ayata C, Dunn AK, Gursoy-Ozdemir Y, Huang Z, Boas DA, Moskowitz MA. Laser speckle flowmetry for the study of cerebrovascular physiology in normal and ischemic mouse cortex. J Cereb Blood Flow Metab. 2004; 24:744–755. [PubMed: 15241182]

Bandyopadhyay R, Gittings AS, Suh SS, Dixon PK, Durian DJ. Speckle-visibility spectroscopy: a tool to study time-varying dynamics. Rev Sci Instrum. 2005; 76:093110.

Boas DA, Dunn AK. Laser speckle contrast imaging in biomedical optics. J Biomed Opt. 2010; 15:011109. [PubMed: 20210435]

Bolay H, Reuter U, Dunn AK, Huang ZH, Boas DA, Moskowitz MA. Intrinsic brain activity triggers trigeminal meningeal afferents in a migraine model. Nat Med. 2002; 8:136–42. [PubMed: 11821897]

Briers JD, Richards G, He XW. Capillary blood flow monitoring using laser speckle contrast analysis (LASCA). J Biomed Opt. 1999; 4:164–75.

Briers JD, Webster S. Quasi real-time digital version of single-exposure speckle photography for full-field monitoring of velocity or flow fields. Opt Commun. 1995; 116:36–42.

Cheng H, Duong TQ. Simplified laser-speckle-imaging analysis method and its application to retinal blood flow imaging. Opt Lett. 2007; 15:2188–90. [PubMed: 17671579]

Cheng HY, Luo QM, Zeng SQ, Chen SB, Cen J, Gong H. Modified laser speckle imaging method with improved spatial resolution. J Biomed Opt. 2003; 8:559–64. [PubMed: 12880364]

Cheng HY, Luo QM, Zeng SQ, Chen SB, Luo WH, Gong H. Hyperosmotic chemical agent's effect on in vivo cerebral blood flow revealed by laser speckle. Appl Opt. 2004; 43:5772–7. [PubMed: 15540434]

Cheng H, Yan Y, Duong TQ. Temporal statistical analysis of laser speckle imaging and its applications to retinal blood-flow imaging. Opt Express. 2008; 16:10214–9. [PubMed: 18607429]

Choi B, Kang NM, Nelson JS. Laser speckle imaging for monitoring blood flow dynamics in the in vivo rodent dorsal skinfold model. Microvasc Res. 2004; 68:143–6. [PubMed: 15313124]

Choi B, Jia W, Channual J, Kelly KM, Lotfi J. The importance of long-term monitoring to evaluate the microvascular response to light-based therapies. J Invest Dermatol. 2008; 128:485–8. [PubMed: 17657245]

Choi B, Ramirez-San-Juan JC, Lotfi J, Nelson JS. Linear response range characterization and in vivo application of laser speckle imaging of blood flow dynamics. J Biomed Opt. 2006; 11:041129. [PubMed: 16965157]

Duncan DD, Kirkpatrick. Can laser speckle flowmetry be made a quantitative tool? J Opt Soc Am A. 2008; 25:2088–94.

Dunn AK, Bolay H, Moskowitz MA, Boas DA. Dynamic imaging of cerebral blood flow using laser speckle. J Cereb Blood Flow Metab. 2001; 21:195–201. [PubMed: 11295873]

Dunn AK, Devor A, Dale AM, Boas DA. Spatial extent of oxygen metabolism and hemodynamic changes during functional activation of the rat somatosensory cortex. Neuroimage. 2005; 27:279–90. [PubMed: 15925522]

Durduran T, Burnett MG, Yu G, Zhou C, Furuya D, Yodh AG, Detre JA, Greenberg JH. Spatiotemporal quantification of cerebral blood flow during functional activation in rat somatosensory cortex using laser-speckle flowmetry. J Cereb Blood Flow Metab. 2004; 24:518–25. [PubMed: 15129183]

Fercher F, Briers JD. Flow visualization by means of single-exposure speckle photography. Opt Commun. 1981; 37:326–30.

Forrester KR, Tulip J, Leonard C, Stewart C, Bray RC. A laser speckle imaging technique for measuring tissue perfusion. IEEETrans Biomed Eng. 2004; 51:2074–84.

Goodman, JW. Statistical Optics. New York: Wiley; 1985.

Hirao M, Oku H, Goto W, Sugiyama T, Kobayashi T, Ikeda T. Effects of adenosine on optic nerve head circulation in rabbits. Exp Eye Res. 2004; 79:729–35. [PubMed: 15500831]

Huang YC, Tran N, Shumaker PR, Kelly KM, Ross V, Nelson JS, Choi B. Blood flow dynamics after laser therapy of port Wine Stain Birthmarks. Lasers Surg Med. 2009; 41:563–71. [PubMed: 19731304]

Jia WC, Choi B, Franco W, Lotfi J, Majaron B, Aguilar G, Nelson JS. Treatment of cutaneous vascular lesions using multiple-intermittent cryogen spurts and two-wavelength laser pulses: numerical and animal studies. Lasers Surg Med. 2007; 39:494–503. [PubMed: 17659588]

Jia W, Sun V, Tran N, Choi B, Liu S, Mihm MC Jr, Phung TL, Nelson JS. Long-term blood vessel removal with combined laser and topical rapamycin antiangiogenic therapy: implications for effective port wine satin treatment. Lasers Surg Med. 2010; 42:105–12. [PubMed: 20166161]

Kirkpatrick SJ, Duncan DD. Detrimental effects of speckle-pixel size matching in laser speckle contrast imaging. Opt Lett. 2008; 33:2886–8. [PubMed: 19079481]

Le TM, Paul JS, Al-Nashash H, Tan A, Luft AR, Sheu FS, Ong SH. New insights into image processing of cortical blood flow monitor using laser speckle imaging. IEEETrans Med Imaging. 2007; 26:833–42.

Liu S, Li P, Luo Q. Fast flow visualization of high-resolution laser speckle imaging data using graphics processing unit. Opt Express. 2008; 16:14321–9. [PubMed: 18794967]

Parthasarathy AB, Tom WJ, Gopal A, Zhang X, Dunn AK. Robust flow measurement with multi-exposure speckle imaging. Opt Express. 2008; 16:1975–89. [PubMed: 18542277]

Ramirez-San-Juan JC, Ramos-García R, Guizar-Iturbide I, Martínez-Niconoff G, Choi B. Impact of velocity distribution assumption on simplified laser speckle imaging equation. Opt Express. 2008; 16:3197–203. [PubMed: 18542407]

Smith TK, Choi B, Ramirez-San-Juan JC, Nelson JS, Osann K, Kelly KM. Microvascular blood flow dynamics associated with photodynamic therapy and pulsed dye laser irradiation. Lasers Surg Med. 2006; 38:532–9. [PubMed: 16615132]

Tom WJ, Ponticorvo A, Dunn AK. Efficient processing of laser speckle contrast images. IEEETrans Med Imaging. 2008; 27:1728–38.

Yuan S, Devor A, Boas DA, Dunn AK. Determination of optimal exposure time for imaging of blood flow changes with laser speckle contrast imaging. Appl Opt. 2005; 44:1823–30. [PubMed: 15813518]

Zhou C, Shimazu T, Durduran T, Luckl J, Kimberg DY, Yu G, Chen XH, Detre JA, Yodh AG, Greenberg JH. Acute functional recovery of cerebral blood flow after forebrain ischemia in rat. J Cereb Blood Flow Metab. 2008; 28:1275–84. [PubMed: 18382471]
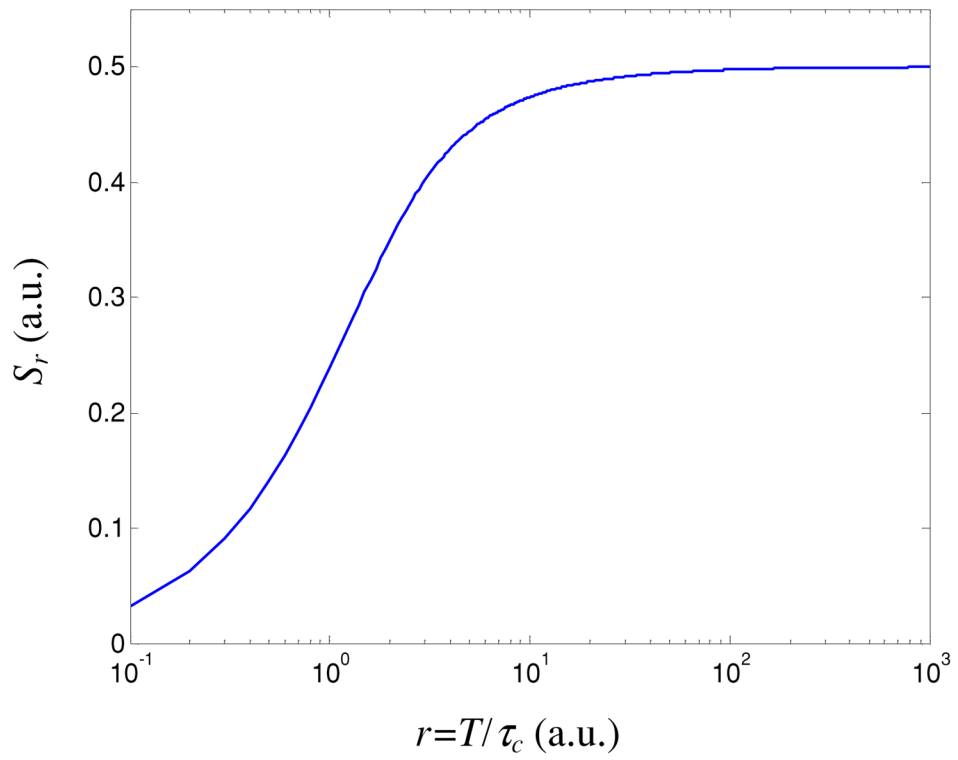
Figure 1.
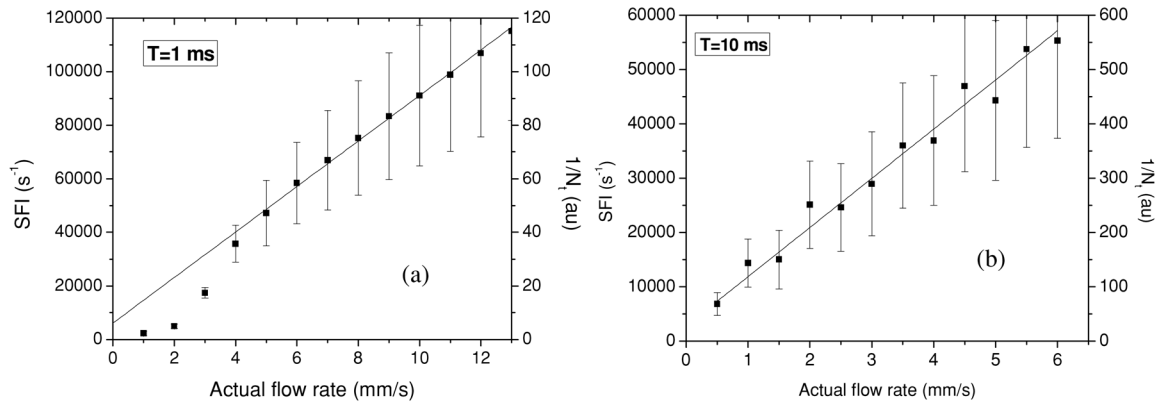Sensitivity as a function of the number of coherence intervals captured over unit of time (i.e. $1/N_t$).

Figure 2.
(a) Both SFI and $1/N_t$ values maintain a linear relationship to the actual flow rate for an actual flow rate greater than 5 mm s^{-1} and an image exposure time of 1 ms. For an actual flow rate less than 5 mm s^{-1}, it is necessary to employ a longer exposure time to achieve a linear response as demonstrated in (b) for $T = 10$ ms.
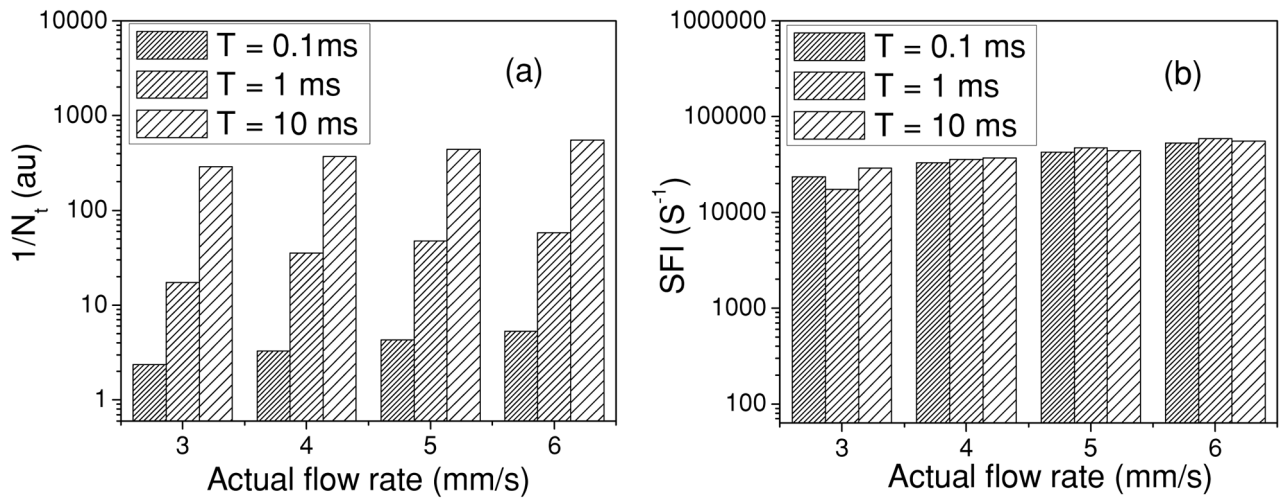
Figure 3.
(a) $1/N_t$ and (b) SFI values as a function of the actual velocity for four exposure times (*T*). Note that, for a given actual flow rate, the $1/N_t$ value depends on exposure time, while the SFI value is unaffected.
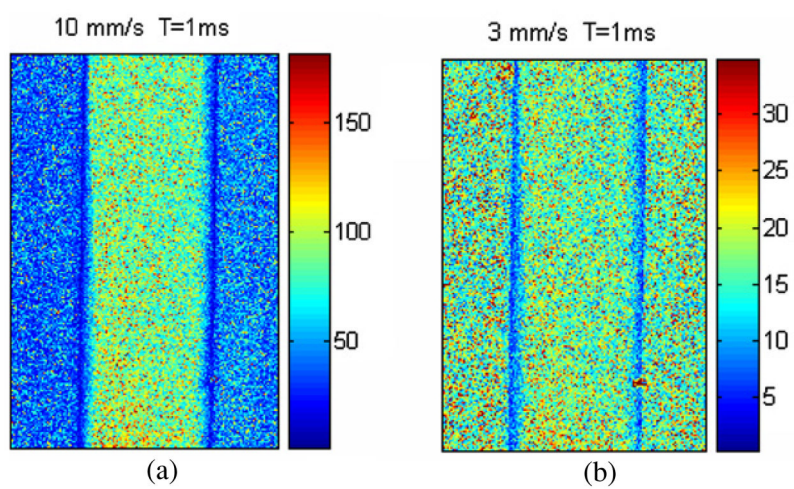
Figure 4.
Maps of *in vitro* flow rates predicted with the mLSI model for actual flow rates of (a) 10 mm s^{-1} and (b) 3 mm s^{-1}.
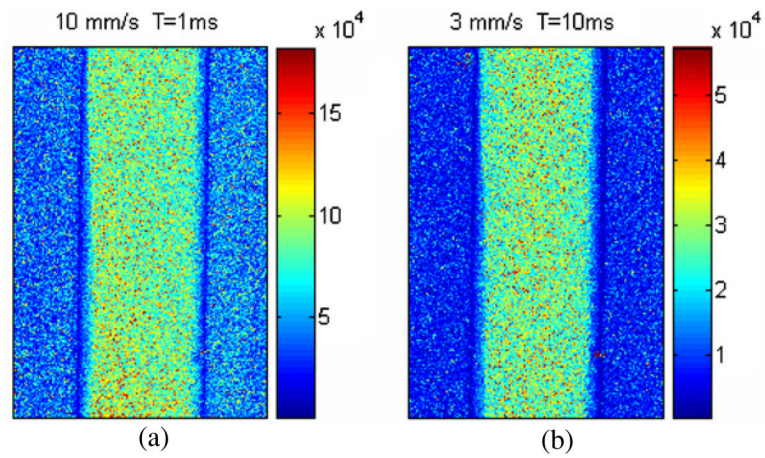
Figure 5.
Maps of *in vitro* flow rate predicted with our mLSI model (equation (5)) for actual flow rates of (a) 10 mm s^{-1} and (b) 3 mm s^{-1}. Exposure times of 1 and 10 ms were used to work within the linear response range of our instrument for the two actual flow rates.

Table 1

Relative flow rate change and % relative error predicted by equations (1) and (6) from figures 4 and 5, respectively.

T (ms)	Flow rate (mm s^{-1})	$1/N_t$ (au)	SFI (s^{-1})
1	10	91.58	91 581
1	3	17.59	N/A[a]
10	3	N/A[b]	28 943
RFVC	10/3 = 3.33	91.58/17.59 = 5.2	91 581/28 943 = 3.16
% relative error	N/A	56.15	5.1

[a]Not applicable because the SFI associated with this exposure time is out of the linear response range.

[b]Not applicable because the parameter $1/N_t$ does not take into account the exposure time.

Table 2

Relative flow rate change and % relative error predicted with equations (1) and (5).

T (ms)	Flow rate (mm s^{-1})	$1/N_t$ (au)	SFI (s^{-1})
1	9	83.491	83 491
1	2	4.907	N/A[a]
10	2	N/A[b]	24 744
RFVC	9/2 = 4.5	83.491/4.907 = 17.01	834 91/24 744 = 3.37
% relative error	N/A	278	25.1

[a]Not applicable because the SFI associated with this exposure time is out of the linear response range.

[b]Not applicable because the parameter $1/N_t$ does not take into account the exposure time.